SAND2014-20344C

# Pulse-Burst PIV in a High-Speed Wind Tunnel

Steven J. Beresh,[1] Sean P. Kearney,[2] Justin L. Wagner,[3] Daniel R. Guildenbecher,[4] John F. Henfling,[5]
Russell W. Spillers,[6] and Brian O. M. Pruett,[7]
*Sandia National Laboratories, Albuquerque, NM, 87185*

Naibo Jiang,[8] Mikhail N. Slipchenko,[9] Jason Mance,[10] and Sukesh Roy[11]
*Spectral Energies LLC, Dayton, OH, 45431*

**Time-resolved particle image velocimetry (TR-PIV) has been achieved in a high-speed wind tunnel, providing velocity field movies of compressible turbulence events. The requirements of high-speed flows demand greater energy at faster pulse rates than possible with the TR-PIV systems developed for low-speed flows. This has been realized using a pulse-burst laser to obtain movies at up to 50 kHz with higher speeds possible at the cost of spatial resolution. The constraints imposed by use of a pulse-burst laser are a limited burst duration of 10.2 ms and a low duty cycle for data acquisition. Pulse-burst PIV has been demonstrated in a supersonic jet exhausting into a transonic crossflow and in transonic flow over a rectangular cavity. The velocity field sequences reveal the passage of turbulent structures and can be used to find velocity power spectra at every point in the field, providing spatial distributions of acoustic modes. The present work represents the first use of TR-PIV in a high-speed ground test facility.**

## Introduction

In recent years, time-resolved particle image velocimetry (TR-PIV) has evolved as a means of measuring temporally correlated velocity fields, allowing the acquisition of PIV movies. Whereas TR-PIV has emerged in a variety of low-speed flows as an adaptation of PIV technology using available commercial kHz-rate lasers and fast CMOS cameras, the requirements of high-speed flows exceed the capabilities of these technologies. Extension beyond roughly 10 kHz is not yet feasible with the diode-pumped solid-state lasers that typically are used in lower speed regimes. Instead, TR-PIV in high-speed flows is best accomplished using a pulse-burst laser, as this is the only light source currently capable of producing sufficient energy at the necessarily rapid pulse rates. Furthermore, it offers the ability to produce pairs of pulses (i.e., doublets) at arbitrary separation times, which allows the very short times between paired exposures compatible with high-speed flow, in contrast with the long time between exposures when using a single sustained kHz-rate laser. Simultaneous with the maturation of pulse-burst laser technology, quality high-speed cameras have begun to achieve desirable framing rates without excessive sacrifice of

[1]Distinguished Member of the Technical Staff, Engineering Sciences Center, AIAA Associate Fellow, correspondence to: P.O. Box 5800, Mailstop 0825, (505) 844-4618, email: sjberes@sandia.gov
[2]Principal Member of the Technical Staff, AIAA Associate Fellow
[3]Senior Member of the Technical Staff, AIAA Senior Member
[4]Senior Member of the Technical Staff, AIAA Member
[5]Distinguished Technologist, AIAA Senior Member
[6]Principal Technologist
[7]Senior Technologist
[8]Research Scientist, AIAA Member
[9]Research Scientist, AIAA Member
[10]Research Scientist, AIAA Member
[11]Senior Research Engineer, AIAA Associate Fellow


This work is supported by Sandia National Laboratories and the United States Department of Energy. Sandia is a multiprogram laboratory managed and operated by Sandia Corporation, a wholly owned subsidiary of Lockheed Martin Corporation, for the United States Department of Energy's National Nuclear Security Administration under contract DE-AC04-94AL85000.

the size of the spatial array.

Pulse-burst PIV has a minimal history. Wernet appears to have been the first to achieve pulse-burst PIV, implementing it in a jet flow at 25 kHz to provide velocity spectra of the turbulent mixing at the interface with ambient air [1]. Recently, Brock et al described their initial efforts to conduct PIV in a supersonic jet using a pulse-burst laser at 1 MHz, but could acquire only short sequences of 13 images and suffered some image degradation [2]. Miller et al demonstrated pulse-burst PIV initially in a small, low-speed jet at 10 kHz [3], then subsequently applied it at 100 kHz to a Mach 0.3 jet. Murphy and Adrian accomplished something similar not using a pulse-burst laser, but by chaining together eight Nd:YAG lasers and cameras to yield sequences of four vector fields at 300 kHz in a blast wave [5]; however, such an approach is necessarily limited in its quantity of frames. Pulse-burst PIV has not seen previous application in a wind tunnel or other testing facility.

The present work represents the first use of pulse-burst PIV in a wind tunnel, and with the exception of those few efforts noted above, the first pulse-burst PIV of any kind. The initial application of pulse-burst PIV has been to a supersonic jet exhausting into a transonic crossflow, building upon earlier investigations by Beresh et al. [6-8]. An additional application to a transonic cavity flow [9, 10] is described as well. Together, these data sets establish the success of pulse-burst PIV in a ground-test facility and its power to investigate the temporal development of turbulent structures in the high-speed flows produced by such a facility.

## Experimental Apparatus

### Wind Tunnel Hardware

Experiments were conducted in Sandia's Trisonic Wind Tunnel (TWT) at Mach 0.8. The TWT is a blowdown-to-atmosphere facility using air as the test gas with interchangeable test sections. For transonic operation, it may be configured with either solid walls or porous walls or some combination thereof. The test section is a straightforward rectangular duct of dimensions 305 × 305 mm$^2$ (12 × 12 inch$^2$) and is enclosed within a pressurized plenum to accommodate ventilated test section configurations. The TWT typically runs for 30-40 seconds at a time with 20-30 minutes between runs.

Two experimental arrangements were used in the present work. The first was a jet in crossflow, in which a supersonic jet was installed on the top wall of the solid-wall transonic test section, identically to previous experiments [6-8]. The jet nozzle was located upstream of the windows to position the imaging region for measurement of the far-field of the jet once it has developed. The laser sheet was introduced through a window in the floor of the test section as well as a matching window in the lower wall of the TWT plenum. It was oriented in the streamwise plane and aligned to the center plane of the test section, which coincided with the center of the jet nozzle exit.

A nitrogen jet exhausted from a conical nozzle with a design Mach number of 3.73, an expansion half-angle of 15 deg, and an exit diameter of 9.53 mm (0.375 inch). In the present case, the jet was operated at a pressure of 3.9 MPa to produce a jet-to-freestream dynamic pressure ratio of $J$=8.1, with the wind tunnel operating at a stagnation pressure $P_0$ of 154 kPa and a fixed stagnation temperature $T_0$ of 321K ± 2K. The coordinate axes originated at the centerpoint of the nozzle exit plane, such that the $u$ component is in the streamwise direction and $v$ component is positive away from the top wall of the tunnel.

A second experiment concerned transonic flow over a rectangular cavity, as in [9, 11]. The cavity is simply a rectangular hole installed into the lower wall of the test section, having dimensions 127 × 127 mm$^2$ (5 × 5 inch$^2$) with a nominal depth of 25.4 mm (1 inch). The test section was configured with porous walls on the top wall and one side wall to alleviate non-physical resonances due to wind tunnel duct modes [11]; a solid wall with a window for imaging was installed in the other side of the test section. A glass floor allowed the laser sheet to enter the cavity from below. The tunnel was operated with $P_0$ = 110 kPa and $T_0$ = 321K ± 2K. The streamwise ($x$), wall-normal ($y$), and spanwise ($z$) coordinate system originated at the spanwise center of the cavity leading edge with $y$ pointed away from the cavity.

The TWT is seeded by a thermal smoke generator (Corona Vi-Count 5000) that produces a large quantity of particles typically 0.2 - 0.3 μm in diameter from a mineral oil base. Particles are delivered to the TWT's stagnation chamber upstream of the flow conditioning section through a series of pipes and tubes, in which agglomeration of the particles occurs. Previous measurement of the *in-situ* particle response across a shock wave generated by a wedge shows the particle size to be 0.7 - 0.8 μm. Stokes numbers have been estimated as at most 0.05 based on *a posteriori* analysis of PIV measurements, which is sufficiently small to rapidly attain the local velocity and reduce particle lag errors to a negligible level.

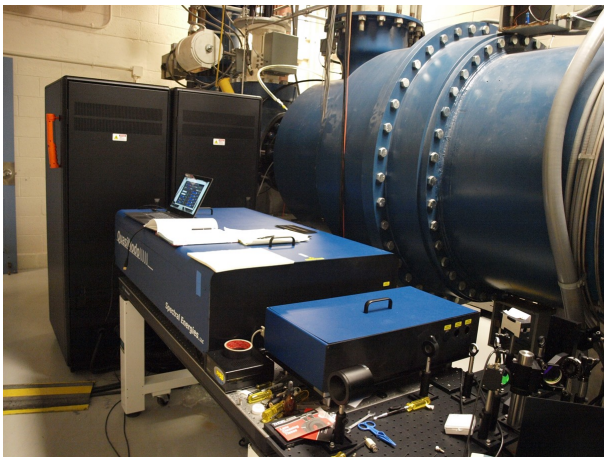

**Fig. 1:** The pulse-burst laser installed adjacent to the Trisonic Wind Tunnel.

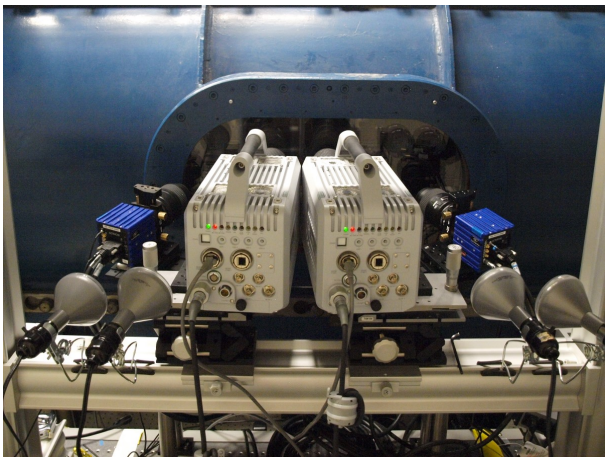

**Fig. 2:** Two high-speed cameras aligned side-by-side for imaging an extended field of view, flanked by two sCMOS cameras for stereoscopic 10-Hz PIV.

**Pulse-Burst PIV System**

A quasi-continuous burst-mode laser (QuasiModo-1000, Spectral Energies, LLC) with both diode- and flashlamp-pumped Nd:YAG amplifiers was used to produce a high energy pulse train at 532 nm. The pulse-burst laser generates up to 10.2 ms duration bursts every 8 seconds with a maximum 532 nm pulse energy of 500 mJ at 5 kHz and 20 mJ pulse energy at its maximum repetition rate of 500 kHz. The laser is capable of producing doublets with variable interpulse spacing at all repetition rates, though in the present work the time between pulses in a doublet was 2.00 μs for the jet-in-crossflow experiment and 2.80 μs for the cavity experiment. Jet-in-crossflow data were acquired using 25 kHz and 50 kHz doublets within a 2.5 ms burst duration with energy per pulse at 532 nm of 175 mJ and 60 mJ, respectively. Cavity data were obtained using 25 kHz doublets within a 10.2 ms burst with pulse energy of 50 mJ. The design of the pulse-burst laser is based on master oscillator power amplifier architecture and is similar to previously reported pulse-burst lasers [12-14]. The laser is shown installed into the wind tunnel in Fig. 1.

Images were acquired using two high-speed CMOS cameras (Photron SA-X2) which have a full framing rate of 12.5 kHz and an array of 1024 × 1024 pixels at this speed. Their windowing function allows the framing rate to be increased by sampling a semi-arbitrary portion of the imaging array. In the present case, each camera operated at 50 kHz with an array of 640 × 384 pixels. Most data were acquired with the two pulses in a doublet frame-straddled around the cameras' interframe transfer time, which allowed cross-correlation analysis of pairs of images; thus PIV velocity fields were acquired at 25 kHz. Additional jet-in-crossflow data were acquired with the laser producing doublets of pulses at 50 kHz that were double-exposed in a single frame for auto-correlation image interrogation. Higher framing rates are possible and easily matched by the pulse-burst laser, but present camera speeds would require undesirable sacrifice of the spatial resolution.

The two cameras were placed side by side as shown in Fig. 2 to extend the field of view in the streamwise direction to track the convection of turbulent eddies using two-component PIV. In the jet-in-crossflow configuration, this yielded a combined field of view of approximately 70 × 21 $mm^2$. Unfortunately, the large size of the camera bodies precluded placing them sufficiently close to one another to image the laser sheet from a normal direction. Therefore, they were canted towards each other at an angle of 5 deg such that their individual imaging regions were adjacent and could seamlessly combine the resulting vector fields. This angle does create a perspective bias on the velocity vectors due to added sensitivity to the out-of-plane velocity component, but calculations estimate that the maximum induced error in the streamwise component is no more than 2%. This was considered to be an acceptable compromise in order to create the desired field of view. The cavity data were acquired similarly but with the cameras moved back to achieve a combined field of view of 103 × 31 $mm^2$, reducing the horizontal cant to 3.5 deg. In addition, they were angled downward by 12 deg to view about 55% into the depth of the cavity. This introduced a larger bias error in the vertical velocity component, estimated to reach as much as 20%; however, past experience has shown that this does not hinder visualization of the cavity flow or detection of turbulent eddies [15].

Also visible in Fig. 2 are two low-speed cameras (LaVision Imager sCMOS) ordinarily used as part of a traditional 10-Hz stereoscopic PIV system. These cameras were installed to acquire additional data using a 10 Hz

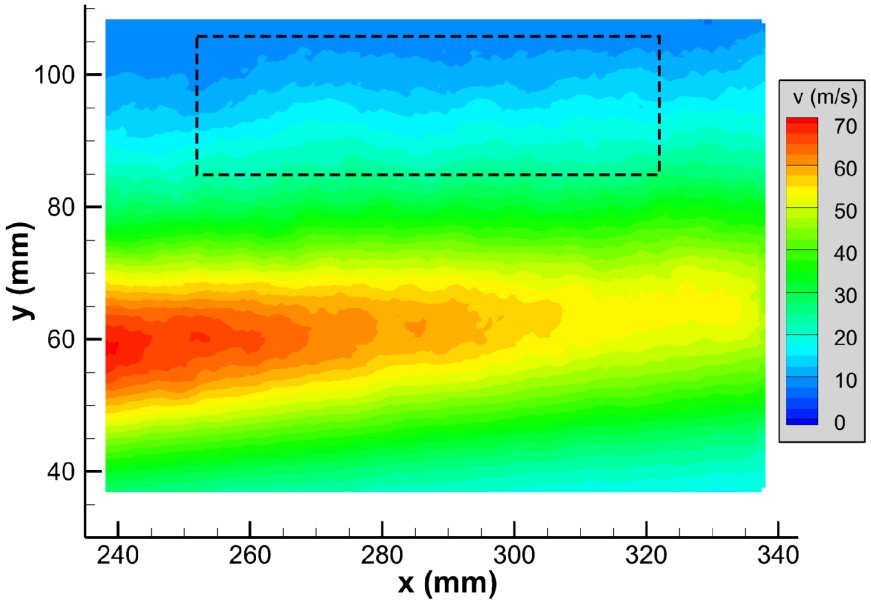


**Fig. 3:** Mean vertical velocity component of the jet in crossflow at Mach 0.8 acquired using a traditional 10-Hz PIV system. The dashed rectangular box illustrates the field of view of the pulse-burst PIV.

laser (Spectra Physics PIV-400), which is better suited to collecting statistical data on the jet in crossflow. These data are largely outside the intended scope of the present article.

Data were processed using LaVision's DaVis v8.2. In each case, image pairs were background-corrected, intensity normalized, and then interrogated with an initial pass using 64 × 64 pixel interrogation windows, followed by two iterations of 24 × 24 pixel interrogation windows. A 50% overlap in the interrogation windows was used as well. The resulting vector fields were validated based upon signal-to-noise ratio, nearest-neighbor comparisons, and allowable velocity range. A single pass of light vector smoothing was employed as well.

## Results

### Jet in Crossflow

A mean velocity field of the vertical velocity component acquired from 1500 independent snapshots of a traditional 10-Hz PIV system is shown in Fig. 3. The field of view was established well downstream of the jet nozzle exit and at some distance from the wall to capture the core of the jet and its mixing interface with the freestream. The strength of the counter-rotating vortex pair is captured by the vertical velocity component and it can be seen to decay with downstream distance as the jet trajectory slowly moves it outward. The dashed rectangular box illustrates the position of the combined field-of-view of the high-speed cameras for the pulse-burst PIV, which is positioned to capture the turbulent eddies to be found at the outward mixing interface. Additional data were acquired nearer to the jet core by raising $J$ to a value of 10.2 and thereby increasing jet penetration into the pulse-burst PIV field of view. The resulting physics at the higher $J$ are more complex and challenging to interpret physically, whereas the present results at $J$=8.1 are more visually comprehensible. Therefore the $J$=8.1 data are well suited to the present demonstration of pulse-burst PIV and the $J$=10.2 data will be discussed in a dedicated future publication. Although TR-PIV frequently has been applied to jet flows, it appears the only application to a jet-in-crossflow configuration prior to the present experiment is Diez et al's experiment in a water tunnel at 1 kHz [16].

A sample velocity field sequence is shown in Fig. 4, acquired at 25 kHz using cross-correlation analysis. It was extracted from a much longer 2.5 ms burst duration and represents only an eight-snapshot, 280-µs portion of the full burst. (A movie of the full sequence may be obtained from the first author of this paper.) The shorter burst duration was chosen over the longer 10.2-ms option to allow greater energy to be imparted into the pulses, which produces superior images on the cameras; this duration is fully sufficient to capture the turbulent mixing events at the jet interface. Velocity fluctuations were found by calculating the mean velocity field over several wind tunnel runs and then subtracting it from each individual velocity field. The plot shows in-plane velocity fluctuations superposed on the derived vorticity field as a color contour and white contour lines denoting the swirl field. The initial time $t$=0 µs is referenced to the start of the full movie sequence. A total of 53 such bursts of PIV data were acquired at $J$=8.1.

Figure 4 shows a counter-rotating pair of eddies entering the field of view on the left edge. As the pair convects downstream, the two eddies can be seen to rotate with respect to one another as they simultaneously drift farther out in the $y$ direction, reflecting the gradual trajectory of the jet. The paired vortices are separated by approximately 10 mm. A second, weaker pair of counter-rotating vortices can be seen to enter the field of view shortly behind the first pair, becoming visible at $t$=1000 μs at the bottom of the frame. Their orientation is nearly horizontal whereas the first pair entered the field of view nearly vertically oriented. These vortices diffuse with downstream travel and become difficult to detect by $t$=1120 μs. Yet another pair of counter-rotating eddies enters the field of view at $t$=1080 μs and still another at $t$=1200 μs, each with different rotational alignment. These paired eddies are characteristic of the entire data set, though their stability varies greatly. Some are like the first pair seen initially at $t$=920 μs in Fig. 4, remaining sharply defined as they convect and rotate. Others may shear one or both of the eddies into smaller eddies or diffuse vorticity, sometimes leading to a single well-defined vortex seen to remain stable and convect downstream intact. Interestingly, each of the eddies within a pair in Fig. 4 is separated by a reasonably consistent 8-10 mm. The distance between pairs is larger, about 20-30 mm.

In addition to the velocity field sequence shown in Fig. 4, data have been acquired with the laser producing pairs of pulses at 50 kHz but without changing the framing rate of the cameras from that used for the previous 25 kHz movies. These doublets were double-exposed on images and then interrogated using auto-correlation analysis. This approach is somewhat noisier and the final interrogation window was set to 32 × 32 pixels rather than 24 × 24 as in the cross-correlations, but was found to be successful because no reverse flow occurs in this flow field. At the cost of spatial resolution and some increase in correlation noise, the sampling rate is therefore doubled.

Figure 5 shows a sequence of six auto-correlated vector fields extracted from the full 2.5 ms burst. (Again, the full movie is available from the first author.) Like Fig. 4, a pair of counter-rotating eddies can be seen entering the field of view at $t$=1700 μs. In this case, however, the eddies are not stable. At $t$=1700 μs, the negative eddy (blue) is diffuse and appears to show two separate but like eddies in the process of coalescing. This process can be observed as time progresses, in which a tighter and stronger positive vortex forms out of the two merging eddies while the two slowly rotate about each other. Meanwhile, the accompanying positive eddy (red) is sheared apart in the process and its vortical strength diminishes markedly during the time sequence. By the final vector field in Fig. 5f, the former pair of vortices has been reduced to essentially a single negative vortex. The higher sampling rate of the auto-correlated data is instrumental in tracking the process of this rapidly evolving event.

Since each velocity vector is a short time sequence, temporal power spectral density (PSD) functions of the velocity fluctuations may be computed. Few previous experiments have sought to measure the energy spectrum of the velocity fluctuations in a jet in crossflow, with most of those efforts devoted to detecting shear layer instabilities in the near-field of a low-speed interaction [17-20]. Energy spectra of the present data are shown in Fig. 6 using the vertical velocity component, assembled from the 53 available bursts of cross-correlated data and again for 25 bursts of auto-correlated data that double the frequency response. Two locations are shown, one upstream within the field of view along the average trajectory of the convecting turbulent eddies and a second downstream location also along the average eddy trajectory.

The peaks of the power spectra in Fig. 6 reside at about 4.5 – 5 kHz for the cross-correlated data and lower at 4 kHz for the auto-correlated data. The lower-frequency peak using the auto-correlated data does not appear to be a function of the frequency resolution because PSD's generated using a doubled resolution did not appreciably shift the peaks. Rather, it likely is an artifact of the poorer spatial resolution of the auto-correlated data, in which larger PIV interrogation windows were necessary. The peak frequency roughly corresponds to twice the distance between pairs of counter-rotating eddies such as observed in Fig. 3, assuming a convection velocity equivalent to the freestream velocity. The correlation noise of the cross-correlated data becomes evident at about 8 kHz and appears to initiate a noise floor, whereas the higher-frequency noise in the auto-correlated data appears at about 15 kHz and continues a trend of diminishing energy as frequency rises.

Figure 6 also suggests that the high-frequency slope may obey a power law of -1; that is, energy is proportional to the inverse of the frequency. If accurate, this would be an unanticipated discovery in turbulent velocity energy spectra. It is well known that within the inertial subrange of turbulence scales, the power-law dependency is -5/3 (e.g., [21]). However, in the present case this regime is unlikely to have been reached by the current temporal capability. A rough estimate based on Kolmogorov scaling indicates the expected onset of the -5/3 slope would be above 20 kHz; adapting Kawai and Lele's simulations [22] suggests about 30 kHz. A -1 dependency at frequencies lower than those of the inertial subrange is well established in pressure power spectra beneath wall-bounded turbulence (e.g., [23]) but its existence in the velocity field remains elusive and controversial [24, 25]. It is unclear whether the present dependency has been located because the jet-in-crossflow physics produce it at lower Reynolds numbers or whether the manifestation of PIV correlation noise and aliasing effects have coincidentally generated an apparent -1 slope. Though these scaling law observations cannot be considered conclusive, the mere ability to

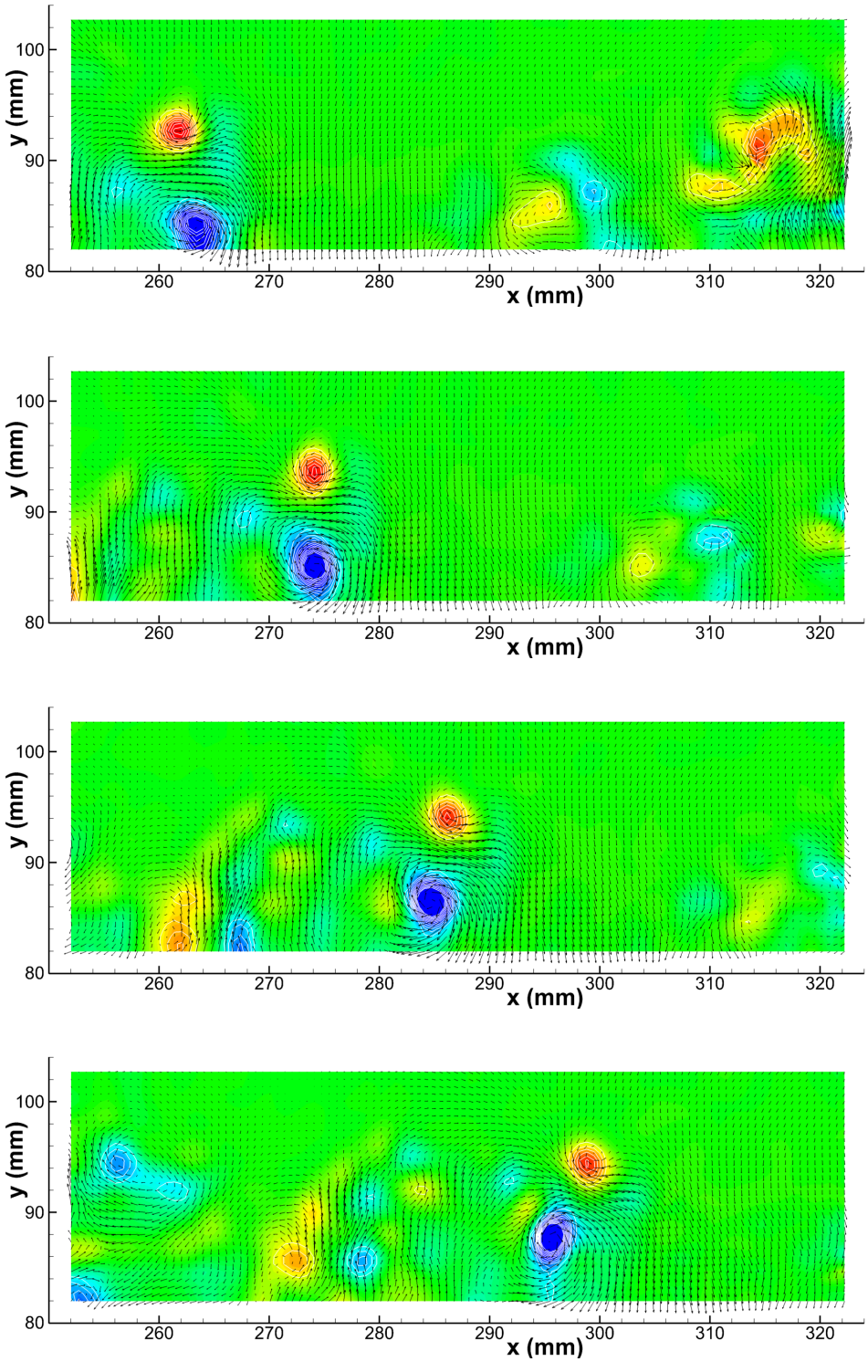


**(a):** t = 920 μs

**(b):** t = 960 μs

**(c):** t = 1000 μs

**(d):** t = 1040 μs

**Fig. 4:** Sequence of eight velocity fields extracted from a 2.5 ms burst of 58 velocity fields acquired at 25 kHz, measuring a Mach 3.7 jet issuing into a Mach 0.8 crossflow at $J$=8.1. Vectors show the in-plane velocity fluctuations superposed on a color contour plot of the derived vorticity field and white line contours of the swirl field. Continued on next page.

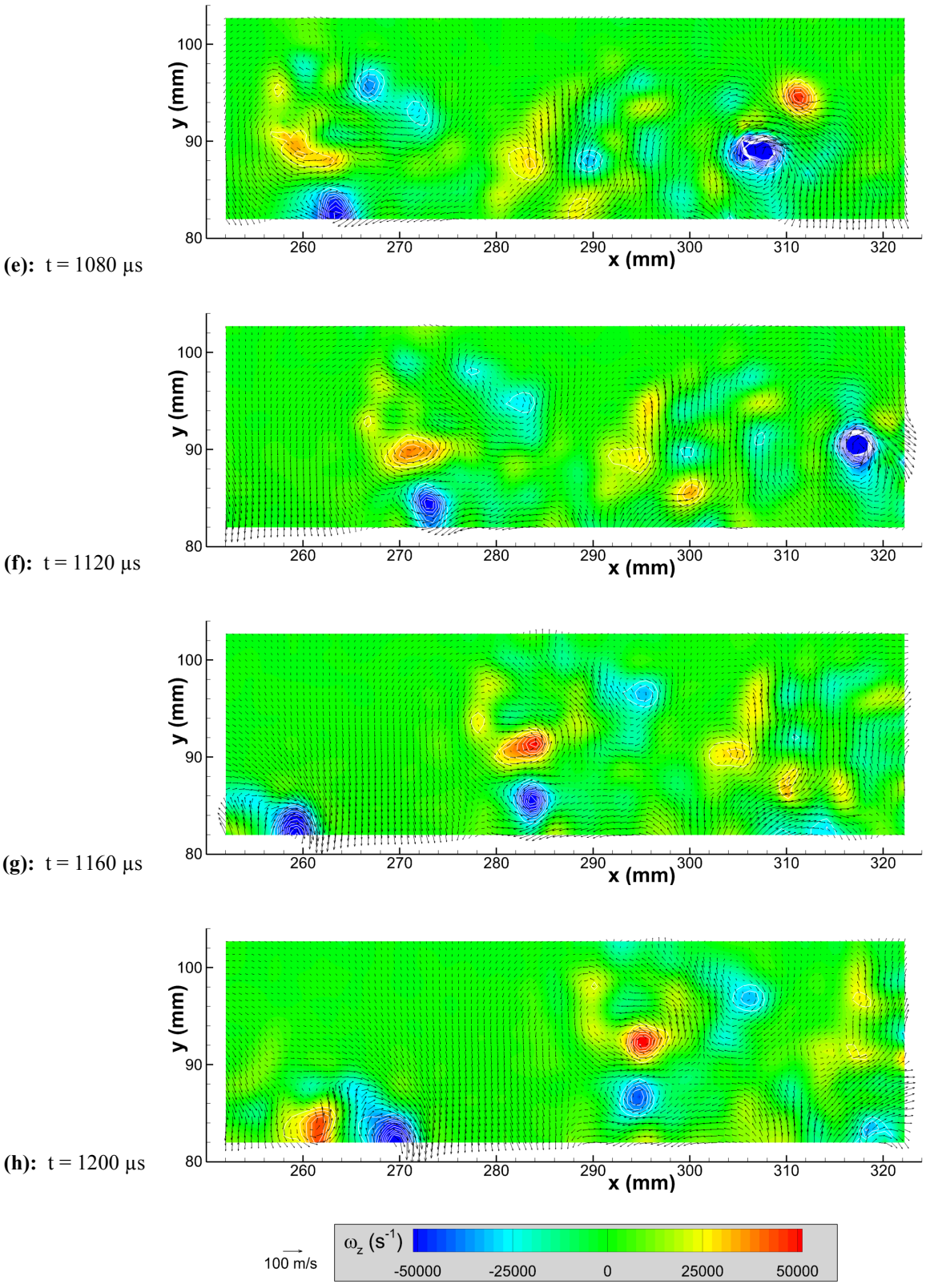


**Fig. 4:** Continued from previous page.

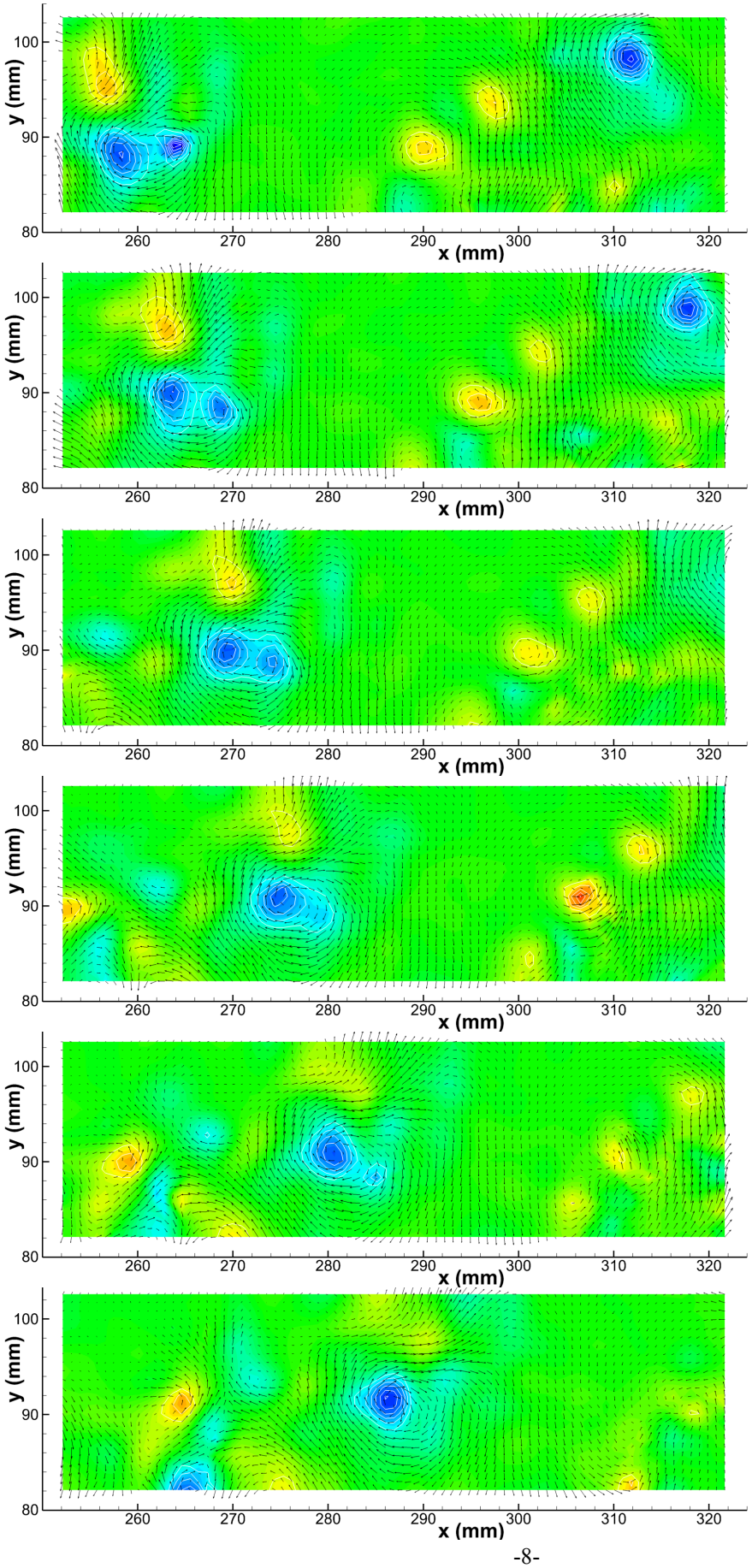


**(a):** t = 1700 µs

**(b):** t = 1720 µs

**(c):** t = 1740 µs

**(d):** t = 1760 µs

**(e):** t = 1780 µs

**(f):** t = 1800 µs

**Fig. 5:** As Fig. 4, but using auto-correlated data at 50 kHz.

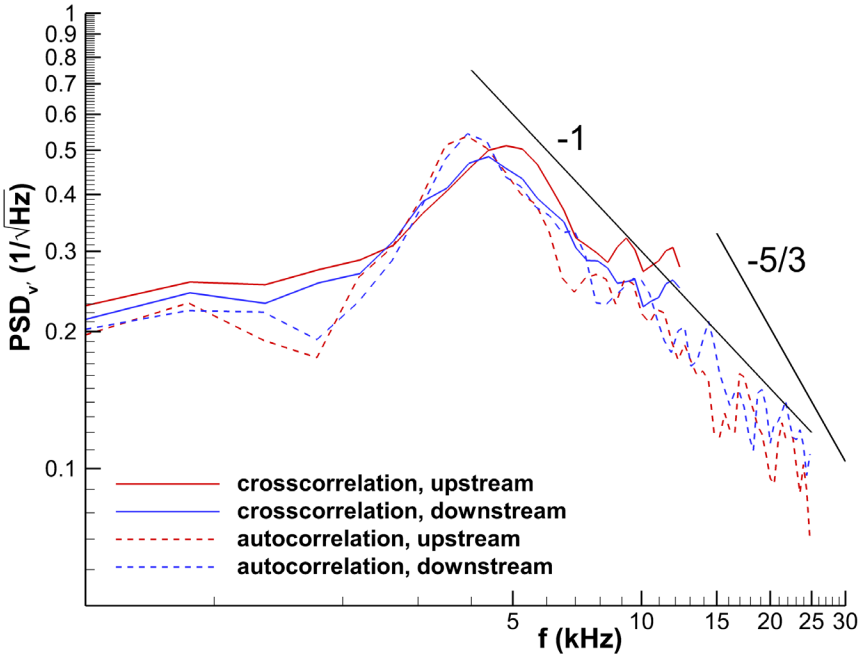


**Fig. 6:** Power spectra of vertical velocity fluctuations found in the jet in crossflow, measured at an upstream location in the field of view ($x$=258 mm, $y$=89 mm) and a downstream location ($x$=313 mm, $y$=93 mm). Includes cross-correlation data at 25 kHz and auto-correlation data at 50 kHz.

examine such high-frequency content in velocity field data acquired in a compressible flow demonstrates the value of pulse-burst PIV.

Considerable additional analysis of the jet-in-crossflow data may be performed to capitalize on the temporal content of pulse-burst PIV, but lies beyond the scope of the current demonstration of capability.

**Rectangular Cavity Flow**

A second demonstration of pulse-burst PIV was accomplished in flow over a rectangular cavity at Mach 0.8, revealing the growth of shear layer structures and their recirculation within the cavity. The behavior of these large-scale structures is key to the acoustic tones produced by the cavity resonance and can be well explored using the temporally correlated velocity fields of pulse-burst PIV. TR-PIV measurements of cavity resonance have been achieved previously in water tunnels [26-28] and in a 4-m/s wind tunnel [29], but never at the high velocities relevant to aircraft aerodynamics.

Two sample velocity field sequences are shown in Figs. 7 and 8. Each offers five snapshots extracted from a 10.2 ms burst of 256 velocity fields acquired at 25 kHz. Vectors show the in-plane velocity fluctuations superposed on a color contour plot of the streamwise velocity component; white line contours portray the vorticity magnitude exceeding a minimum threshold to emphasize the strongest regions of shear and turbulent eddies. In each figure, the positions of the cavity walls coincide with the axes shown in (e), thus locating the field of view. As discussed subsequently, neither figure follows a uniform time progression; instead snapshots are chosen at appropriate time steps to illustrate important fluid dynamic events. Movies of the full sequences may be obtained from the first author and the times marked in Figs. 7 and 8 are referenced to the start of the movie sequences.

Figure 7 portrays a strong ejection event at the aft end of the cavity. The first four frames are separated by 120 μs each, which actually encompasses three vector fields and therefore subsamples the framing rate by a factor of three. At the start of the sequence, a weak vortex is visible at the aft corner of the cavity with a strong recirculation region upstream of it lifting flow off the cavity floor (roughly 70 mm < $x$ < 110 mm). Meanwhile, a shear layer vortex ($x \approx 70$ mm, $y \approx 5$ mm) is incident towards this region. By $t$ = 8680 μs, the vortex has encountered the uplifted recirculating flow and is diverted upwards and begins to shear apart ($x \approx 80$ mm, $y \approx 5$ mm). The interaction of the incoming vortex and the recirculation region creates a significant outward motion in the shear layer that resembles a wave crest, whose outward motion continues in the third frame at $t$ = 8800 μs. The outbound velocities of this crest continue to intensify at $t$ = 8800 μs ($x \approx 110$ mm, $y \approx 10$ mm) and produce the ejection of flow

from the cavity. At this point, the recirculation region has shifted upstream within the cavity (reaching about $x$ = 100-105 mm) and flow near the aft wall also shows outbound motion to join with the ejection event associated with the cresting shear layer. The final frame in Fig. 7e occurs 600 μs later and has been selected to show how greatly the structure of the recirculation region has changed following the ejection. At this time, recirculating fluid has moved well upstream but without reaching to the aft wall (terminating at about $x$ = 65-70 mm) and fluid from the shear layer dives down into the aft end of the cavity. A caveat should be noted in that the velocity field does not reach the cavity floor and motion nearer the floor may contradict the vectors available.

The velocity field snapshots of Fig. 8 have been selected to track the lifetime of a single exemplary shear layer vortex. The five snapshots were chosen to depict important stages in its life and therefore do not follow a uniform progression in time. At $t$ = 4520 μs, the vortex in question may be seen to enter the field of view at $x \approx 35$ mm; the vortex location suggested by the vorticity contours and the velocity vectors may not align perfectly because the ideal convective reference frame is not portrayed in the vector plot. At the same time, a strong recirculation event is occurring in the streamwise center of the plot and it interacts with the shear layer vortices. This is evident in the full movie sequence, which shows that the vortices at $x \approx 70$ mm and $x \approx 80$ mm in Fig. 8a originate in the shear layer and are deflected over the top of the recirculation region. The vortex at $x \approx 35$ mm, on the other hand, experiences a different fate. In Fig. 8b, at $t$ = 4720 μs, it has encountered the front of the recirculation event ($x \approx$ 45-50 mm) and although the vorticity contours suggest it is stretched by this circumstance, the velocity vectors indicate it remains strongly coherent. By $t$ = 5040 μs, its downstream progression has slowed ($x \approx 55$ mm), it has been pressed lower into the cavity, and the vortex remains at the leading front of the recirculation event, all while retaining a strong rotational identity. At $t$ = 5160 μs, it has scarcely advanced, pinned in place by the recirculation region; its immobility is particularly evident in the movie. The final snapshot shows the vortex trapped in the same location with its vortical strength greatly diminished, and the movie shows its continued destruction over the next several frames.

As with the jet-in-crossflow data, the 36 bursts of cavity PIV data may be analyzed for frequency content by finding the power spectra of the velocity fluctuations. In Fig. 9, the PSD of the vertical velocity component is shown for two positions in the flow, one measured above the shear layer and one within the core of the shear layer; both were positioned at $x$=76.8 mm, a little beyond the streamwise midpoint of the cavity length. Also shown in Fig. 9 is a PSD of the pressure fluctuations recorded by a high-frequency pressure sensor (Kulite XCQ-062) installed in the aft cavity wall at $y$=-10.7 mm on spanwise center. Four acoustic tones are clearly seen in the pressure spectrum, corresponding to the first four Rossiter tones in the cavity. Although the mode 1 tone at $f$=620 Hz is only weakly present in the two velocity spectra, modes 2 through 4 are clearly evident and well match the pressure frequencies; even the bifurcated peak of the mode 4 pressure tone is visible in the velocity spectra, particularly the one obtained within the shear layer. The velocity peaks are broadened in comparison with the pressure peaks because the velocity PSD's were computed using a frequency resolution of 100 Hz, whereas the faster sampling rate of the pressure data allowed a resolution of 10 Hz. The tone amplitudes are stronger within the shear layer but do not have the same prominence as in the spectrum measured above the shear layer. This is because the broadband fluctuations are an order of magnitude higher inside the shear layer where turbulent fluctuations are very strong, whereas the flow above the shear layer experiences predominantly acoustic perturbations.

Though Fig. 9 shows velocity power spectra for only two points in the flow, similar spectra are available for every velocity vector recorded. This means that pulse-burst PIV provides the spatial distribution of the acoustic mode amplitudes and can identify locations where acoustic loading will be most intense. To this purpose, the PSD amplitudes of modes 1 through 3 are shown in Fig. 10 for the vertical velocity component. Figure 10a shows that the mode 1 resonance is tied to the recirculation region, while Figs. 10b and 10c reveal that modes 2 and 3 originate within the shear layer. Mode 2 additionally is concentrated within the streamwise center of the shear layer whereas mode 3 extends across its entire length. This provides insight into the fluid dynamical origin of the resonances as well as mapping the loading environment within the cavity.

The pulse-burst PIV data of the cavity flow were obtained simultaneously with pressure signals from high-frequency sensors mounted in the forward and aft walls of the cavity. Numerous data analysis approaches are made possible, including pressure-velocity correlations, velocity movies bandpass-filtered for specific resonance tones, and dynamic mode decomposition for spectral analysis. Although the scope of such analyses necessitates a dedicated article, the present demonstration of pulse-burst PIV establishes the new possibilities for the experimental study of turbulent flows in a high-speed ground test facility.

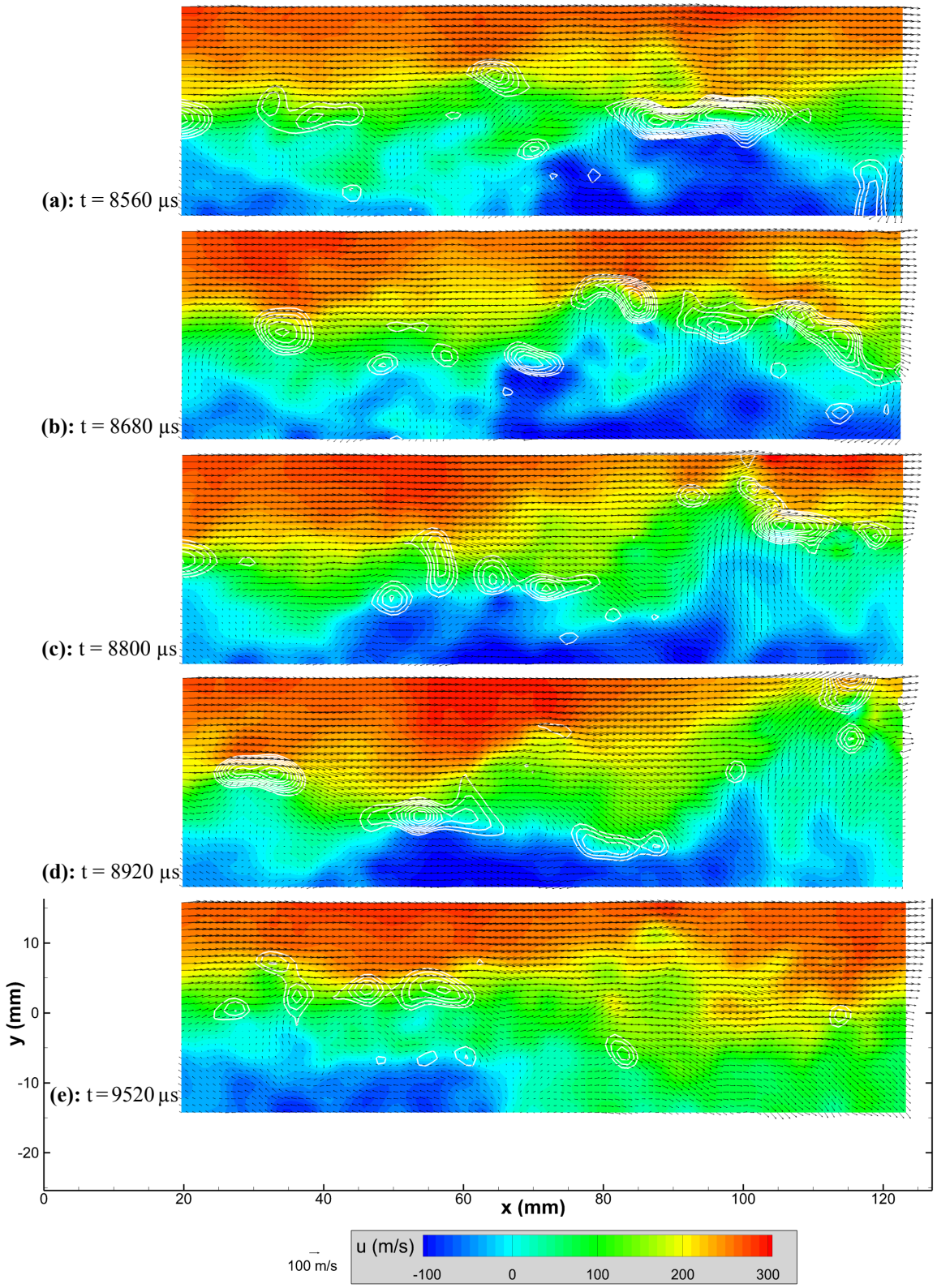


**Fig. 7:** Sequence of velocity fields extracted from a 10.2 ms burst of 256 velocity fields acquired at 25 kHz, measuring flow over a rectangular cavity at Mach 0.8. Vectors show the in-plane velocity fluctuations superposed on a color contour plot of the streamwise velocity component and white line contours of the vorticity magnitude exceeding a minimum threshold. The axes in (e) coincide with the positions of the cavity walls. Note that (e) is a later-time snapshot out of progression with (a) – (d).

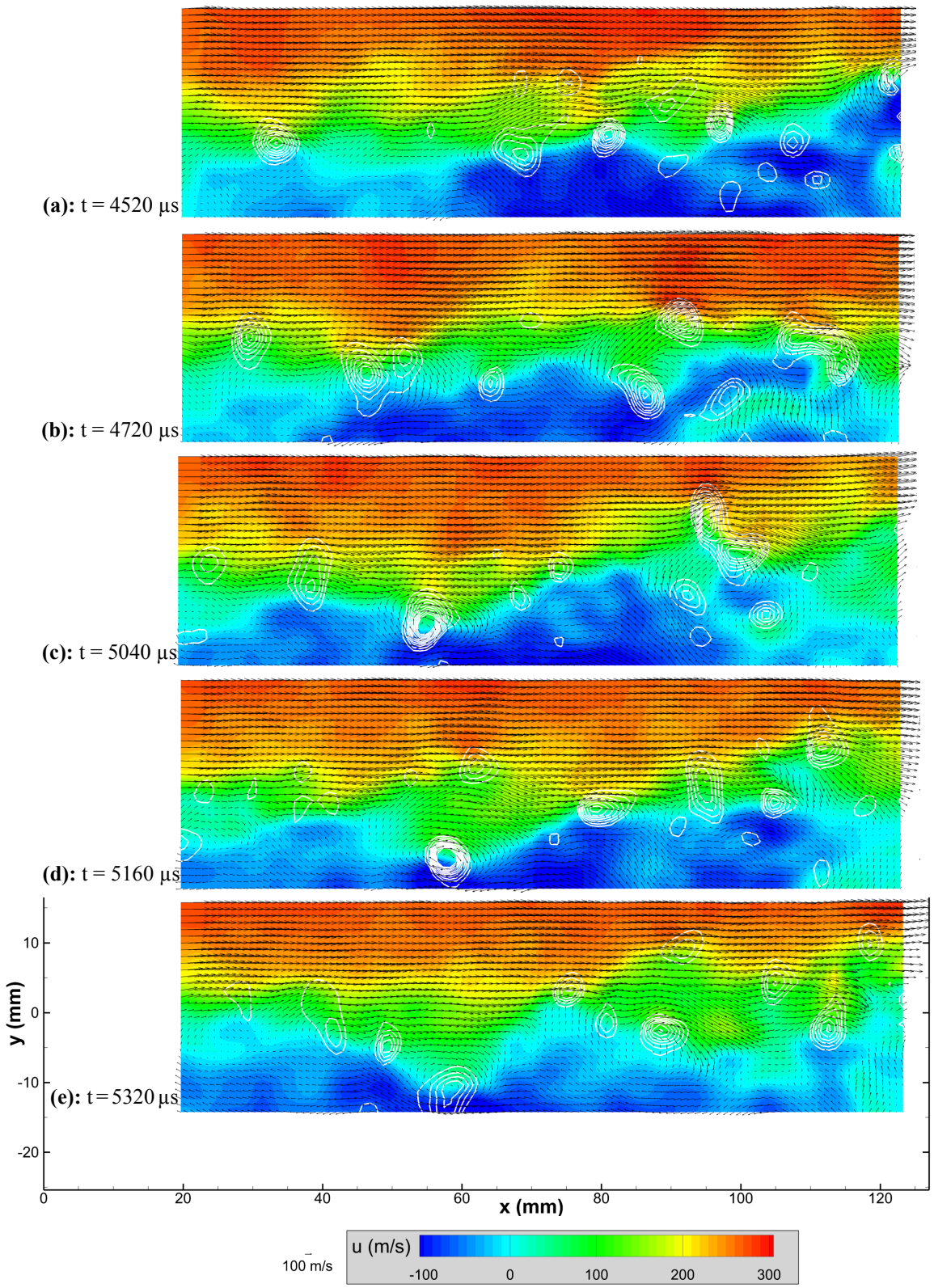


**Fig. 8:** Sequence of velocity fields extracted from a 10.2 ms burst of 256 velocity fields acquired at 25 kHz, measuring flow over a rectangular cavity at Mach 0.8. Vectors show the in-plane velocity fluctuations superposed on a color contour plot of the streamwise velocity component and white line contours of the swirl field. The axes in (e) coincide with the positions of the cavity walls. Note that snapshots do not follow a uniform progression in time.

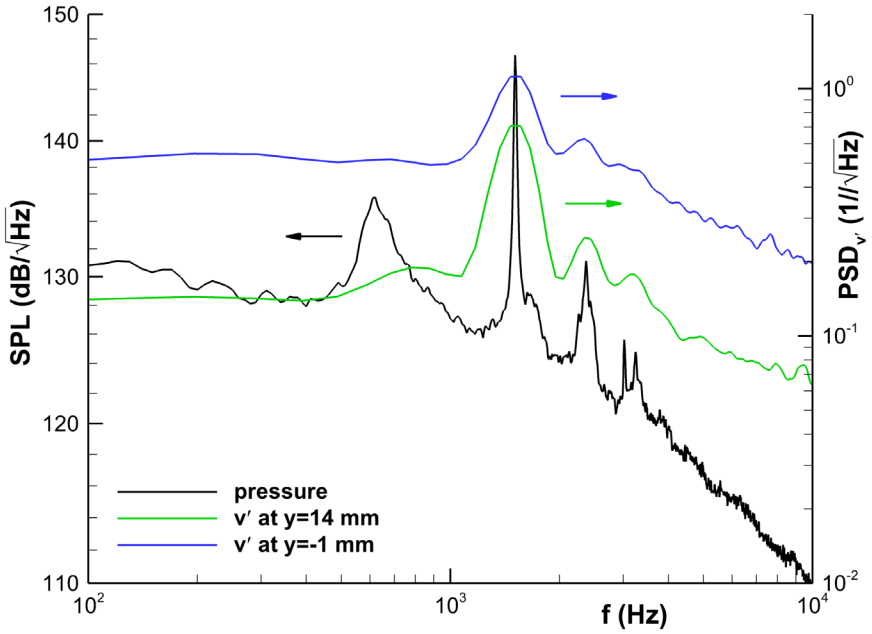


**Fig. 9:** Power spectra of vertical velocity fluctuations found in the cavity flow, measured above the shear layer ($x$=76.8 mm, $y$=14 mm) and within the shear layer ($x$=76.8 mm, $y$=-1 mm). Also shown is a PSD of the pressure data measured by a sensor in the aft cavity wall at the spanwise center.

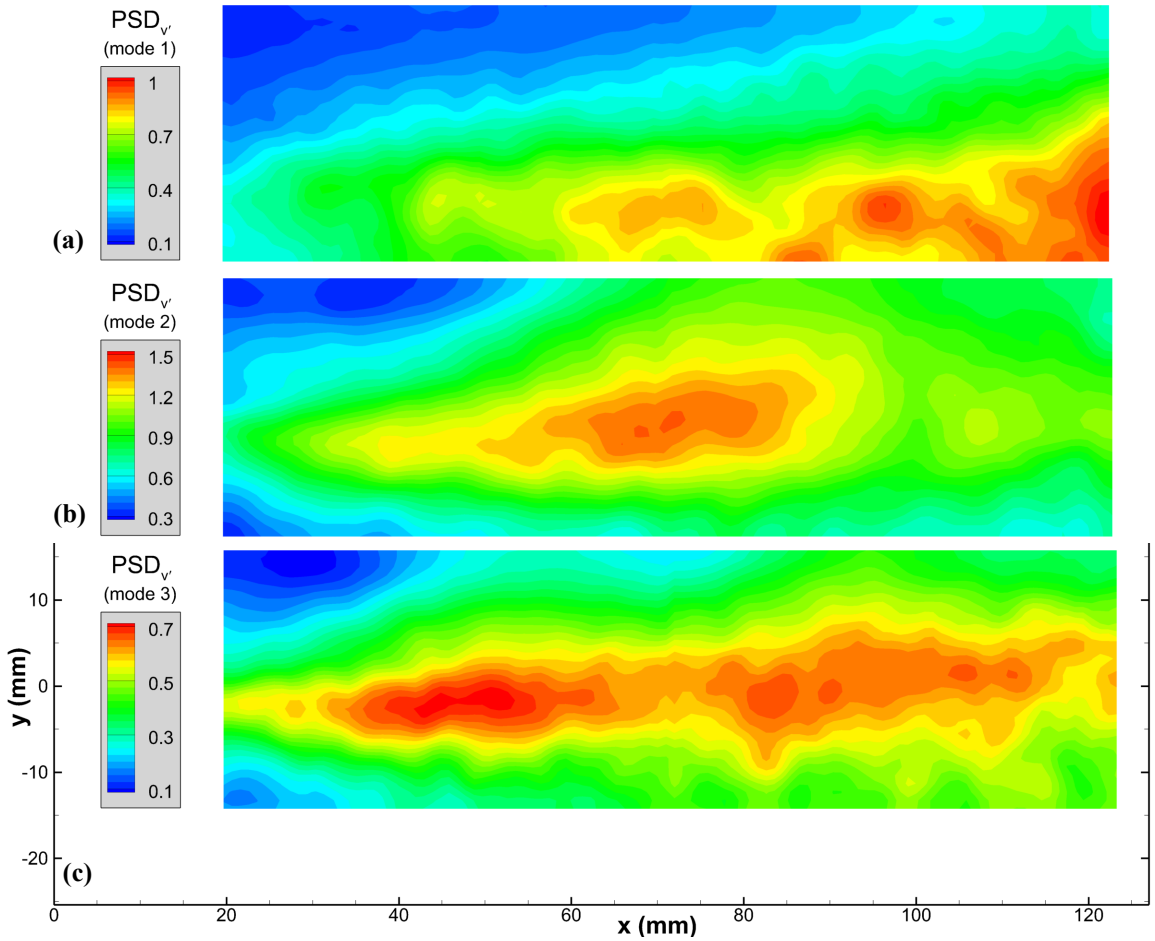


**Fig. 10:** Spatial distribution of power spectral density amplitudes of vertical velocity fluctuations at specific frequencies corresponding to acoustic tones; (a) mode 1 (f=620 Hz); (b) mode 2 (f=1510 Hz); (c) mode 3 (f=2380 Hz).

## Conclusion

Time-resolved particle image velocimetry (TR-PIV) has been achieved in a high-speed wind tunnel through the use of a pulse-burst laser, providing velocity field movies of compressible turbulence events. Although TR-PIV may be achieved in low-speed flows up to roughly 10 kHz using commercial diode-pumped solid-state lasers, the requirements of high-speed flows demand greater energy at faster pulse rates. This has been realized using a pulse-burst laser to obtain sequences at up to 50 kHz with higher speeds possible at the cost of spatial resolution. The constraints imposed by use of a pulse-burst laser are a limited burst duration of 10.2 ms and a low duty cycle for data acquisition. The present work represents the first use of TR-PIV in a high-speed ground test facility and establishes its power to investigate the temporal development of turbulent structures in compressible flows.

Pulse-burst PIV has been demonstrated in a supersonic jet exhausting into a transonic crossflow and in transonic flow over a rectangular cavity. The jet-in-crossflow data reveal the passage of turbulent eddies at the mixing interface of the jet in the far-field of the interaction. Such eddies are often found to occur in counter-rotating pairs though other instances show vortices of common sign coalescing into a larger vortex or instances of a stronger vortex shearing apart a weaker vortex of opposite sign. The cavity data show the flapping of the shear layer and its influence on flow at the aft end of the cavity, as well as the variety of events to which turbulent vortices may be subjected. Velocity power spectra have been calculated at every point in the field, revealing prominent acoustic resonance modes that are consistent with simultaneous pressure data from a sensor in the aft cavity wall. The spatial distributions of the mode amplitudes provide insight into the origin of the resonances and map the resulting loading environment. Numerous further analyses of the time-correlated data are possible.

## References


[1] Wernet, M., "Temporally Resolved PIV for Space-Time Correlations in Both Cold and Hot Jet Flows," *Measurement Science and Technology*, Vol. 18, No. 5, 2007, pp. 1387-1403.

[2] Brock, B., Haynes, R. H., Thurow, B. S., Lyons, G., and Murray, N. E., "An Examination of MHz Rate PIV in a Heated Supersonic Jet," AIAA Paper 2014-1102, January 2014.

[3] Miller, J. D., Michael, J. B., Slipchenko, M. N., Roy, S., Meyer, T. R., and Gord, J. R., "Simultaneous High-Speed Planar Imaging of Mixture Fraction and Velocity using a Burst-Mode Laser," *Applied Physics B*, Vol. 113, 2013, pp. 93-97.

[4] Miller, J. D., Gord, J. R., Meyer, T. R., Slipchenko, M. N., Mance, J. G., and Roy, S., "Development of a Diode-Pumped, 100-ms Quasi-Continuous Burst-Mode Laser for High-Speed Combustion Diagnostics," AIAA Paper 2014-2524, June 2014.

[5] Murphy, M. J., and Adrian, R. J., "PIV Space-Time Resolution of Flow behind Blast Waves," *Experiments in Fluids*, Vol. 49, No. 1, pp. 193-202, 2010.

[6] Beresh, S. J., Henfling, J. F., Erven, R. J., and Spillers, R. W., "Penetration of a Transverse Supersonic Jet into a Subsonic Compressible Crossflow," *AIAA Journal*, Vol. 43, No. 2, 2005, pp. 379-389.

[7] Beresh, S. J., Henfling, J. F., Erven, R. J., and Spillers, R. W., "Turbulent Characteristics of a Transverse Supersonic Jet in a Subsonic Compressible Crossflow," *AIAA Journal*, Vol. 43, No. 11, 2005, pp. 2385-2394.

[8] Beresh, S. J., Henfling, J. F., Erven, R. J., and Spillers, R. W., "Crossplane Velocimetry of a Transverse Supersonic Jet in a Transonic Crossflow," *AIAA Journal*, Vol. 44, No. 12, 2006, pp. 3051-3061.

[9] Wagner, J. L., Beresh, S. J., Casper, K. M., Pruett, B. O. M., Spillers, R. W., and Henfling, J. F., "Experimental Investigation of Aspect-Ratio Effects in Transonic and Subsonic Rectangular Cavity Flows," AIAA Paper 2014-1446, January 2014.

[10] Beresh, S. J., Wagner, J. L., Pruett, B. O., Henfling, J. F., and Spillers, R. W., "Supersonic Flow over a Finite-Width Rectangular Cavity," *AIAA Journal*, 2014, doi: http://arc.aiaa.org/doi/abs/10.2514/1.J053097.

[11] Wagner, J. L., Casper, K. M., Beresh, S. J., Pruett, B. O. M., Spillers, R. W., and Henfling, J. F., "Mitigation of Wind Tunnel Wall Interactions in Subsonic Cavity Flows," AIAA Paper 2014-3026, Atlanta, GA, June 2014.

[12] Slipchenko, M. N., Miller, J. D., Roy, S., Gord, J. R., Danczyk, S. A., and Meyer, T. R., "Quasi-Continuous Burst-Mode Laser for High-Speed Planar Imaging," *Optics Letters*, Vol. 37, No. 8, pp. 1346-1348, 2012.

[13] Slipchenko, M. N., Miller, J. D., Roy, S., Gord, J. R., and Meyer, T. R., "All-Diode-Pumped Quasi-Continuous Burst-Mode Laser for Extended High-Speed Planar Imaging," *Optics Express*, Vol. 21, No. 1, pp. 681-689, 2013.

[14] Slipchenko, M. N., Miller, J. D., Roy, S., Meyer, T. R., Mance, J. G., and Gord, J. R., "100-kHz, 100-ms, 400-J Burst-Mode Laser with Dual-Wavelength Diode Amplifiers," *Optics Letters*, Vol. 39, No. 16, pp. 4735-4738, 2014.

[15] Beresh, S. J., Wagner, J. L., and Pruett, B. O. M., "Particle Image Velocimetry of a Three-Dimensional Supersonic Cavity Flow," AIAA Paper 2012-0030, Nashville, TN, January 2012.

[16] Diez, F. J., Torregrosa, M. M., and Pothos, S., "A Comparison Between Round Turbulent Jets and Particle-Laden Jets in Crossflow by Using Time-Resolved Stereoscopic Particle Image Velocimetry," *Journal of Fluids Engineering*, Vol. 133, No. 9, 2011, pp. 091301.

[17] Moussa, Z. M., Trischka, J. W., and Eskinazi, S., "The Near Field in the Mixing of a Round Jet with a Cross-Stream," *Journal of Fluid Mechanics*, Vol. 80, Part 1, 1977, pp. 49-80.

[18] Andreopoulos, J., "On the Structure of Jets in a Crossflow," *Journal of Fluid Mechanics*, Vol. 157, 1985, pp. 163-197.

[19] Fric, T. F., and Roshko, A., "Vortical Structure in the Wake of a Transverse Jet," *Journal of Fluid Mechanics*, Vol. 279, 1994, pp. 1-47.
[20] Megerian, S., Davitian, J., Alves, L. S. de B., and Karagozian, A. R., "Transverse-Jet Shear-Layer Instabilities. Part 1. Experimental Studies," *Journal of Fluid Mechanics*, Vol. 593, 2007, pp. 93-129.
[21] Pope, S. B., *Turbulent Flows*, Cambridge University Press, 2000, pp. 228-239.
[22] Kawai, S., and Lele, S. K., "Large-Eddy Simulation of Jet Mixing in Supersonic Crossflows," *AIAA Journal*, Vol. 48, No. 9, 2010, pp. 2063-83.
[23] Bull, M. K., "Wall-Pressure Fluctuations Beneath Turbulent Boundary Layers: Some Reflections on Forty Years of Research," *Journal of Sound and Vibration*, Vol. 190, No. 3, 1996, pp. 299-315.
[24] Perry, A. E., Henbest, S., and Chong, M. S., "A Theoretical and Experimental Study of Wall Turbulence," *Journal of Fluid Mechanics*, Vol. 165, 1986, pp. 163-199.
[25] Nickels, T. B., Marusic, I., Hafez, S., and Chong, M. S., "Evidence of the $k_1^{-1}$ Law in a High-Reynolds-Number Turbulent Boundary Layer," *Physical Review Letters*, Vol. 95, No. 7, 2005, pp. 074501.
[26] Haigermoser, C., Vesely, L., Novara, M., and Onorato, M., "A Time-Resolved Particle Image Velocimetry Investigation of a Cavity Flow with a Thick Incoming Turbulent Boundary Layer," *Physics of Fluids*, Vol. 20, 2008, pp. 105101.
[27] Bian, S., Driscoll, J. F., Elbing, B. R., and Ceccio, S. L., "Time Resolved Flow-Field Measurements of a Turbulent Mixing Layer over a Rectangular Cavity," *Experiments in Fluids*, Vol. 51, No. 1, 2011, pp. 51-63.
[28] Liu, X., and Katz, J., "Vortex-Corner Interactions in a Cavity Shear Layer Elucidated by Time-Resolved Measurements of the Pressure Field," *Journal of Fluid Mechanics*, Vol. 728, 2013, pp. 417-457.
[29] Basley, J., Pastur, L. R., Lusseyran, F., Faure, T. M., and Delprat, N., "Experimental Investigation of Global Structures in an Incompressible Cavity Flow using Time-Resolved PIV," *Experiments in Fluids*, Vol. 50, No. 4, 2011, pp. 905-918.